Hindawi
Science and Technology of Nuclear Installations
Volume 2018, Article ID 3106039, 12 pages
https://doi.org/10.1155/2018/3106039

Research Article

Analysis of Steam Explosion under Conditions of Partially Flooded Cavity and Submerged Reactor Vessel

Sang Ho Kim, Seong-Wan Hong, and Rae-Joon Park

Thermal Hydraulic and Severe Accident Research Division, Korea Atomic Energy Research Institute, 989-111 Daedeok-daero, Yuseong-gu, Daejeon 34057, Republic of Korea

Correspondence should be addressed to Sang Ho Kim; sangho@kaeri.re.kr

Received 21 March 2018; Revised 21 May 2018; Accepted 6 June 2018; Published 5 July 2018

Academic Editor: Arkady Serikov

A steam explosion in a reactor cavity makes a mechanical load of the pressure pulse, which can result in a failure of the containment isolation. To prove the integrity of the containment during the ex-vessel steam explosion, the effects of water conditions on a steam explosion have to be identified, and the impulse of a steam explosion has to be exactly assessed. In this study, the analyses for steam explosions were performed for the conditions of a partially flooded cavity and a submerged-vessel in a pressurized water reactor. The entry velocity of a corium jet for the scale of the test facility was varied to simulate the two plant conditions. The TEXAS-V code was used for simulating the phases of premixing and explosion, and the load of a steam explosion was estimated based on the pressure variation. The impulse of a steam explosion under the condition of a corium jet falling into water without a free-fall height is bigger than that under a free-fall height. The fragmented mass of corium in an explosion phase and the distribution of steam fraction are the main parameters for the total load of the steam explosion. This study is expected to contribute to analyses of a steam explosion for a severe accident management strategy.

1. Introduction

The safety of a nuclear power plant is becoming increasingly important over time. The release of radioactive materials has to be prevented for the safety of the public and environment even during a core-melt accident. Immediately after the Fukushima accidents, many countries established a policy for beyond design basis and severe accidents.

Korea enacted a law regarding severe accidents in 2016. It includes the need for an analysis for the factors that can threaten the integrity of the containment after remarkable core damage. A molten fuel-coolant interaction (FCI) was specified as one of the threat factors in the notice. An ex-vessel steam explosion (SE) can occur when a reactor vessel (RV) is broken, and molten-corium falls into the water in the reactor cavity. To show the capability of maintaining the integrity of the containment for the steam explosion, the dynamic pressure from the steam explosion has to be estimated and the structural analysis for the dynamic load on the containment has to be performed.

To resolve the remaining FCI issues for light water reactors, there was a representative international cooperation program of SERENA (Steam Explosion REsolution for Nuclear Applications) in two phases. The scope of the SERENA Phase-1 Program focused on assessing the predictive capabilities of existing tools for reactor cases [1]. The SERENA Phase-1 Program concluded that one variable was not sufficient to explain the level of the loads. In addition, it was emphasized that the uncertainties on a variable distribution in premixing had to be reduced, and the complex effects of variables on steam explosion energetics had to be clarified [1]. The scope of the Phase-2 program focused on resolving the remaining uncertainties through performing complementary analytical work and confirmatory testing [2]. The program also included the reactor calculations defined as the reference cases for a boiling water reactor and a pressurized water reactor. In a comparison with the Phase-1 program, better consistency of most of the results was noticed by various models. The roles of melt fragmentation and solidification, the impact of void on the intensity of an explosion, and

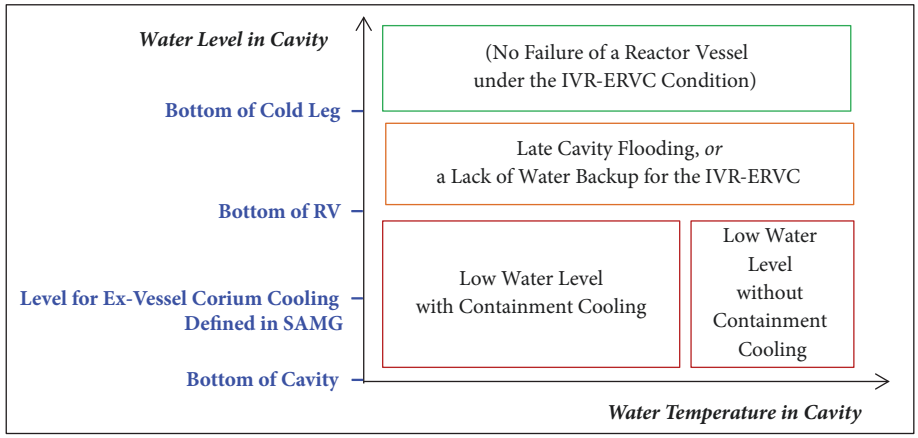

Figure 1: Water conditions in cavity and causes of the conditions when a reactor vessel fails.

the triggering mechanisms were emphasized as the major outcomes of the SERENA-2 program [3].

The understanding and knowledge of the overall phenomenon of steam explosion have been discussed and gathered in a recent status report on ex-vessel steam explosion [4]. Technical opinions on the variables of the scenario conditions, phenomenon model parameters, and the main properties were gathered and investigated comprehensively for each importance and status of knowledge. It had been decided by the experts to rank the key phenomena and their possible consequences at a reactor. Jet fragmentation in water, melt droplet characteristics, melt solidification, melt oxidation, fine fragmentation, and stratified configuration have been considered as being important and having medium or insufficient knowledge.

To resolve the relationship between main parameters and a steam explosion load, various researches have recently been carried out in many institutions. Li et al. studied jet breakup length and fragmentation behavior which directly affect the ultimate strength of a steam explosion [5]. The result showed that melt temperature had strong impact on fragmentation that needs to be embodied in advanced fragmentation models. Zhong et al. used a multiphase code with the volume of fluid method to simulate the earlier behavior of droplet when vapor film exited at the phases of triggering and propagation in steam explosion [6]. The paper concluded that vapor film had little effect on the hydrodynamic droplet deformation when the intensity of the pressure pulse was very high.

For an ex-vessel steam explosion load in a typical PWR cavity geometry, Moriyama and Park studied the probability distribution of steam explosion loads in terms of uncertainties in the model parameters and initial conditions [7]. Six uncertainty parameters, the melt inlet diameter and velocity, initial melt temperature, water pool depth, melt droplet diameter during premixing, and the triggering time were chosen and modeled by probability profiles. The loads were strongly correlated with the premixed mass as an intermediate variable, which depended primarily on the melt jet inlet diameter. The water depth showed nearly linear impact on the potential load. Based on the results of the parametric analyses, a simplified method for evaluation of the steam explosion load was proposed and the results from the proposed method showed fair agreement with JASMINE code [8].

The actual initial conditions of an ex-vessel steam explosion analysis are divided into two kinds according to the procedure in a severe accident management guideline (SAMG) of each plant in Korea. First, in conventional PWRs such as the OPR1000 (Optimized Power Reactor 1000 MWe), the cavity must be filled with water to prevent a containment basemat melt-through by molten-corium concrete interaction in the cavity after a reactor vessel is ruptured. Therefore, there is a reference water level for sufficient ex-vessel coolability of the corium layer. The water is filled to a specific level below the bottom of the reactor vessel. Under this condition, the corium discharged from a reactor vessel falls freely through the air and reaches the surface of the water in the cavity; from here, this is called a "partially flooded cavity condition." Second, in advanced PWRs such as the APR1400 (Advanced Power Reactor 1400 MWe), AP1000 (Advanced Passive 1000 MWe in Westinghouse), and SMART (System-integrated Modular Advanced ReacTor), an IVR-ERVC (in-vessel corium retention through external reactor vessel cooling) strategy is adopted for cooling the corium inside a reactor vessel, resulting in protection of the integrity of a reactor vessel. The strategy is carried out by filling the cavity with water to the level of the cold leg bottom. The reactor vessel is submerged, and heat from the corium is transferred to the water outside the reactor vessel. It is a fully flooded condition in the cavity; from here, this is called a "submerged-RV condition." Even though the IVR-ERVC strategy has sufficient safety margins after setting the condition, there is a possibility of a failure for performing the strategy. Figure 1 shows the water conditions in the cavity and the causes of the levels and temperatures of the water in the cavity when a reactor vessel fails.

The ex-vessel steam explosion is wholly dependent on cavity water conditions based on the cavity flooding procedures during a severe accident. First, the effect of the corium entry condition has to be considered under partially flooded cavity and submerged-RV conditions. An entering velocity of

a jet into water is related to the fragmentation of a melt jet in water. Second, the effects of the water levels and temperatures have to be considered in terms of a steam explosion. The water level in the cavity is a factor directly determining the amount of corium contributing to the load of a steam explosion. The water temperature is a factor needed to be considered in calculating the void fraction at each water height.

The purpose of this paper is to analyze the effects of the free-fall of corium on a steam explosion by benchmarking previous experimental cases. Two premixing experiments presenting partially flooded cavity conditions and submerged-RV conditions in the TROI (Test for Real cOrium Interaction with water) facility were modeled by the TEXAS-V code. The experimental results were utilized for validations of the simulations in the premixing phase. Based on the validated results in the premixing phases of the two conditions, the explosion phases were additionally calculated by the TEXAS-V code and analyzed.

2. Analysis Method

2.1. Simulation Code. The TEXAS-V code developed at the University of Wisconsin-Madison was used for simulating a steam explosion [9]. TEXAS-V has transient, three-fluid, and one-dimensional models capable of simulating fuel-coolant mixing interactions [10]. For the vapor and liquid fields of water, there are mass, momentum, and energy equations as the governing equations in the code. For the Lagrangian fuel particle field, momentum and energy equations are included in the code. Three hydraulic fragmentation models are included in the code. They are Rayleigh-Taylor instabilities (RTI), Kelvin-Helmholtz instabilities (KHI), and boundary layer stripping (BLS).

The phases of the premixing, triggering, propagation, and expansion in a steam explosion are simulated by the TEXAS-V code. After the simulation for the premixing of liquid particles and water in a defined period of time, a triggering is assumed to occur at a defined location for the simulation of a steam explosion. In other words, the defined trigger pressure is imposed on the specific water node in the code. The shock wave from the triggering pressure causes the collapse of the vapor film around each fuel particle. The fragmented corium particles are rapidly quenched owing to direct contact with water. It causes the vaporization of water around the particles. The increased amount of vapor increases the local pressure within a very short time. Finally, the increased pressure sustains the shock wave propagation to neighboring regions. The propagation and expansion phases of the steam explosion in the TEXAS-V were modeled based on this continuous process. When a void fraction is larger than the limit constant in a cell of the TEXAS-V, it is regarded that the direct contact area between the fuel particles and water is small. It means less film collapse and vapor generation. Therefore, the fragmentation rate in the propagation phase sharply decreases as a void fraction increases.

Validation of TEXAS-V has been carried out by utilizing experimental programs including FARO, KROTOS, and TROI test facilities. The TEXAS-V computer code was reviewed by the code developers and shown to be quite capable if simulating the complete vapor explosion process from mixing to the explosion propagation and expansion [11]. Annunziato et al. found that TEXAS application to FARO and KROTOS test cases revealed reasonable prediction capabilities following the optimization of certain input parameters such as heat transfer coefficient for forced convection film boiling for quenching tests and limiting void fraction and fragmentation time for explosion tests [12]. Chen et al. also found that the melt jet leading front position and steam volume during the mixing process predicted by the TEXAS code showed good agreement with the KS-2 and KS-4 experimental data in the KROTOS facility as the coarse mixing status up to the explosion triggering time was well predicted [13]. Song et al. reviewed the capabilities and deficiencies of the fundamental models of the TEXAS-V in terms of their adequacy in a simulation of steam explosion on a reactor scale by evaluating the steam explosion model against the experimental data of KROTOS-44, FARO L-33, TROI-13, and TROI-34 [14, 15]. The experimental cases (TROI-68 and TROI-79) were used to analyze the effects of the free-fall distance on the steam explosion for a subsequent simulation of a reactor case in this paper [16, 17].

2.2. Simulation Conditions. The experiments of TROI carried out in Korea were utilized for analyzing the effects of the water level and free-fall distance on the premixing of the corium particles.

The two experiments presenting partially flooded cavity conditions and submerged-RV conditions were simulated using TEXAS-V, and the results of the experiments and codes were compared. The first experiment (TROI-68) represents the partially flooded cavity condition. Figure 2 shows the TROI facility used to simulate partially flooded reactor cavity conditions. Molten materials are released by gravity with a 1 m free-fall distance between the corium release nozzle and water surface in the test section. This condition indicates that the water level is lower than the level of the reactor vessel bottom. This can take place owing to the insufficient amount of water in carrying out the IVR-ERVC strategy or the original strategy of the ex-vessel corium cooling using the cavity flooding system as a preflooding concept.

The second experiment (TROI-79) represents the submerged-RV condition filling the cavity with the water up to the level of the cold leg. Figure 3 shows the experimental facility for the reactor-submerged conditions. As there is no free-fall of corium, the corium is directly discharged into the water in the test section. It was set for analyzing the effect of no free-fall distance between the release valve and water under the IVR-ERVC condition.

In the two experiments, the main conditions remained the same, excluding the free-fall distance of corium. Table 1 shows the initial test conditions of the TROI-68 and TROI-79. The corium consisted of 80% UO2 and 20% ZrO2. The temperature of the corium was tuned to be about 3,000 K. About 20 kg of corium was released to the interaction vessel. 360 kg of water in 341 K was placed in the test section below the corium release nozzle in the two experiments. The test

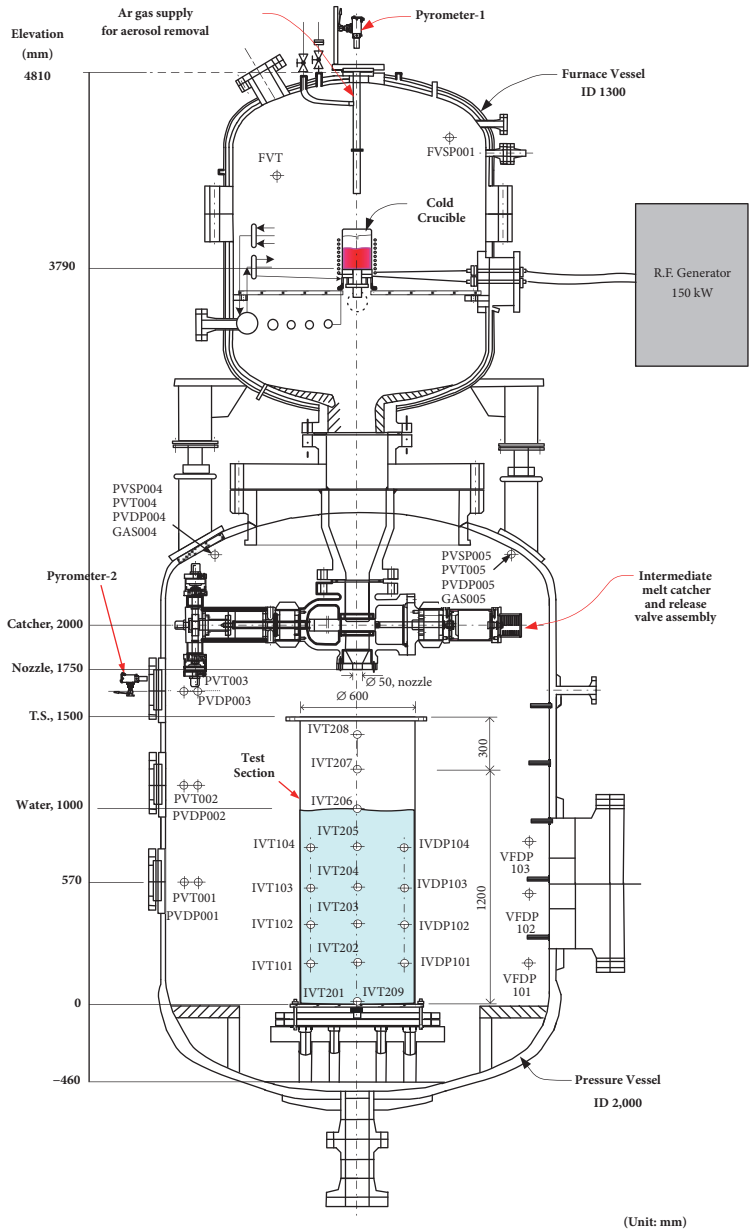

Figure 2: Schematics of TROI-68 experimental facility for partially flooded cavity.

section was a square water tank whose height and area were 1.0 m and 0.36 m^2. The detailed conditions and results of the experiments were described in the previous papers [16, 17]. In the simulations, the code input was set up according to the properties and conditions of the tests.

The results of the premixing phase in the code are compared with the experimental data in the next chapter. Based on the simulation results of the premixing phase, the cases including the explosion phases were simulated to analyze the effects of corium entry condition on the impulse of the steam explosion. The main phenomenon parameters in the sensitivity analyses are explained in Table 2. The values used for the reference case and the values in each case of sensitivity analysis are specified. The sensitivity analyses for the premixing phases in the two experimental cases are done and explained in each subchapter.

3. Simulations for Premixing Phase

3.1. Partially Flooded Cavity Condition. First, the TROI-68 experiment for the partially flooded cavity condition is simulated by the code.

Location variations of the melt jet leading front in the condition for a partially flooded cavity are shown in Figure 4. In the TROI experiment, thermocouples were installed along the centerline of the test section for detecting the location of the melt front with time. The red-filled circles were marked in Figure 4 at each midpoint where the detected temperature

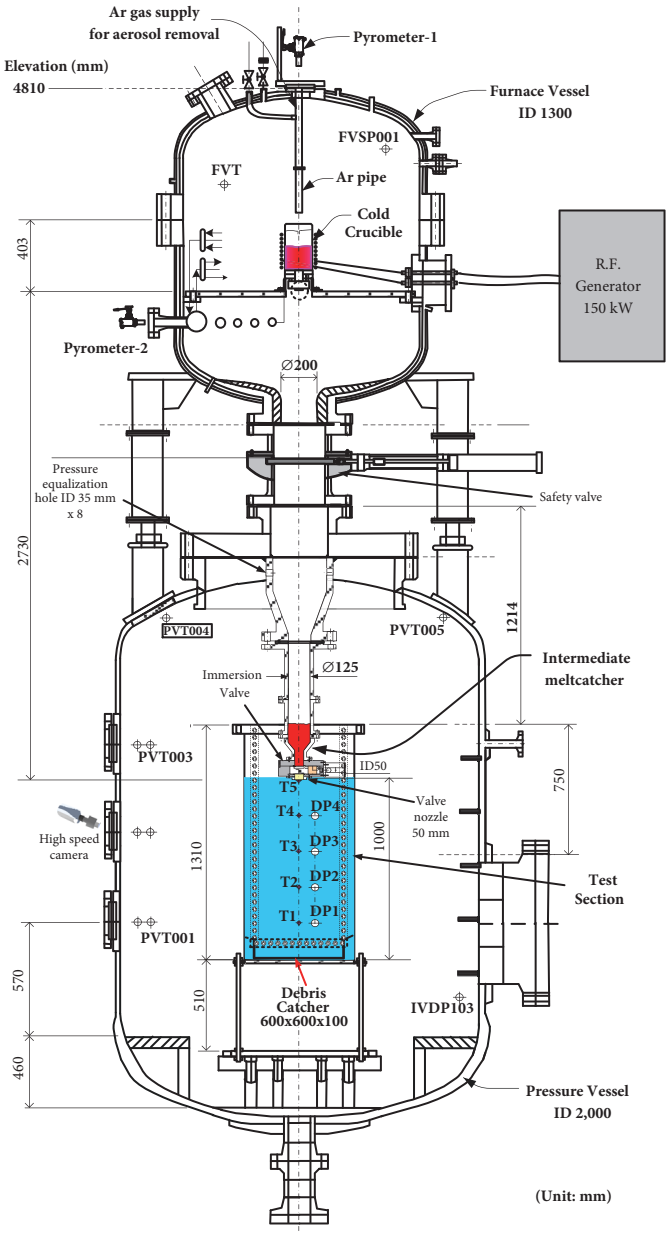

Figure 3: Schematics of TROI-79 experimental facility for submerged-RV.

sharply increased. In addition, as the side section of this experiment was recorded by a video camera, the location of the melt front could be observed in one direction. The results observed through the camera were marked with blue-filled squares. In the TEXAS-V simulation, the initial melt velocity at the intermediate nozzle was set to be almost zero. Owing to the acceleration through a 1 m free-fall, the entering velocity of the melt jet was 4.35 m/s at the water level. In both the experiment and simulation, the strong fragmentation from Rayleigh-Taylor instability caused by the high velocity of the melt jet resulted in the sharp decrease of the jet velocity during 0.3 s after entering the water.

A sensitivity analysis for the parameters of the premixing phase in the TEXAS-V code was performed. Figure 5 shows the main results of the sensitivity analyses. The relative convergence criteria for liquid and gas mass equations were first checked and there was no change in the calculation results. When the coherent jet entry model with a trailing edge was applied, the melt jet and free particles were regarded to be independent of each other for fragmentation in a mesh cell. As the frontal part of the melt jet was continuously fragmented, the time for reaching the bottom was delayed. When the coherent jet entry model with a leading edge was applied, the melt jet front was fragmented by taking over the free particles. In the reference case, the fragmentation was modeled using RTI, KHI, and BLS. There was no big difference in the melt jet front location in the premixing phase when the initial and minimal bubble and droplet radius and

Table 1: Initial conditions in TROI tests.

	TROI-68	TROI-79
Melt		
UO2/ZrO2 (wt%)	80:20	80:20
Temperature (maximum) (K)	2990	3015
Charged mass (kg)	29.58	34.30
Released mass (kg)	19.18	22.54
Plug/puncher diameter (cm)	10.0 / 8.5	10.0 / 8.5
Jet diameter (cm)	5.0 (nozzle)	5.0 (nozzle)
Nozzle–to–water surface distance (m)	1	-0.01 (below the water)
Test section		
Water mass (kg)	360	360
Water pool depth (cm)	100	100
Cross section (m2)	0.36	0.36
Initial temperature (K)	341	341
Pressure vessel		
Initial pressure (air) (MPa)	0.205	0.125
Initial temperature (K)	307	311

Table 2: Cases and parameters in sensitivity analysis.

Name of Case	Description for Parameter in Sensitivity Analysis	Reference Value	Value in Sensitivity Analysis
REF	*(Reference case)*	-	-
Trailing Edge	Particle injection mode & break-up model flag	RTI, KHI, BLS	coherent jet entry model with trailing edge
Leading Edge	Particle injection mode & break-up model flag	RTI, KHI, BLS	coherent jet entry model with leading edge
NB-#	The Number of leading particles	4.0 (Partially Flooded case), 1.0 (Submerged-RV case)	1.0 – 5.0

KHI coefficient changed. As the number of leading particles increased, the time for reaching the bottom was delayed owing to the fragmentation on each particle being regarded as independent.

In the TROI experimental facility, four K-type thermocouples were installed to measure the water temperature at heights of 0.2, 0.4, 0.6, and 0.8 m on the side wall of the test section. When the melt jet front reached the bottom of the test section, the temperature of the water rose by about 1.0 K at the 0.4 and 0.6 m thermocouples in the experiment. On the other hand, the temperature of the water rose by 2.0 K in the code. It is the averaged value in the cell as the TEXAS-V is a one-dimensional code. Even though the center of the cell is highly heated owing to the fragmented corium particles, the heat is transferred to the whole water inside the cell. In Figure 6, the similar tendency of void fractions is shown in the TROI experiment and TEXAS-V simulation. Many small bubbles around the fragmented corium particles were observed in the experiment. The void fractions increased due to the increase of the total heat transfer area between melt particles and water by the fragmentation of the melt particles. At the time the corium reached the bottom, the void fraction in the center of the water was 0.20 in the TROI experiment and 0.24 in the TEXAS-V code. The distribution of void fractions in the premixing phase plays a significant role in the thermal fragmentation in the propagation phase.

3.2. Submerged-RV Condition. Second, the TROI-79 experiment for the submerged-RV condition is simulated by the code.

Location variations of the melt jet leading front in the condition for submerged-RV condition are shown in Figure 7 with the results of a sensitivity analysis. In the TROI experimental facility, five thermocouples were installed at each height of the test section for detecting the location of melt jet front and measuring the velocity. There were 26 thermocouples in total. The red circles with the bars were marked by the first one, which showed the earliest temperature increase among the five thermocouples. The error bars represented the start and end of the temperature increase in the thermocouple. In the TEXAS-V simulation, the initial melt velocity at the intermediate nozzle was assumed to be the same as in the simulation for the partially flooded cavity condition.

In the sensitivity analysis, there was no difference in the results from the change of the calculation criterion of the code. The options for the fragmentation models did not affect

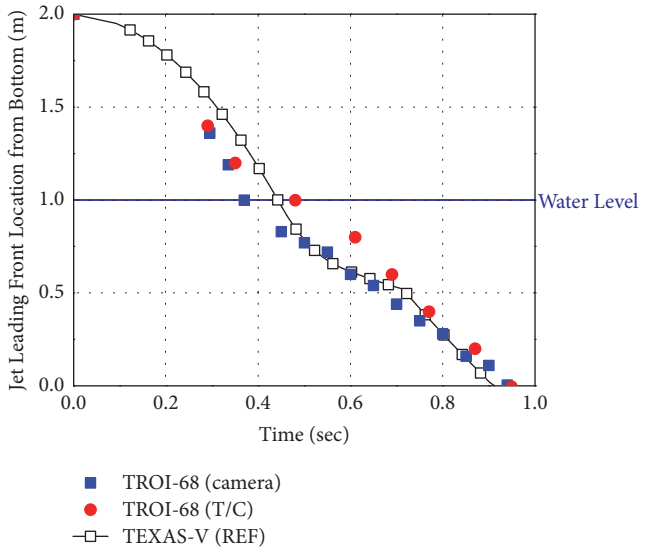

FIGURE 4: Locations of melt jet leading front in TROI experiment and TEXAS-V simulation for the partially flooded cavity condition.

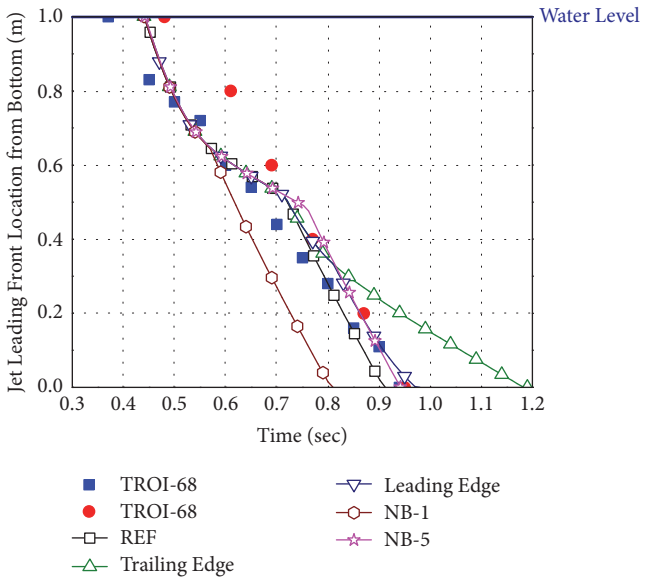

FIGURE 5: Results of sensitivity analysis for melt particle locations in partially flooded cavity condition.

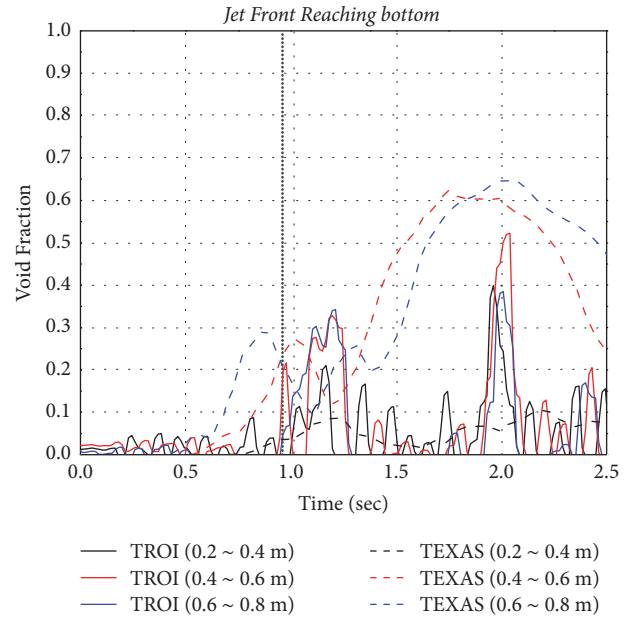

FIGURE 6: Void fractions in TROI experiment and TEXAS-V simulation for the partially flooded cavity condition.

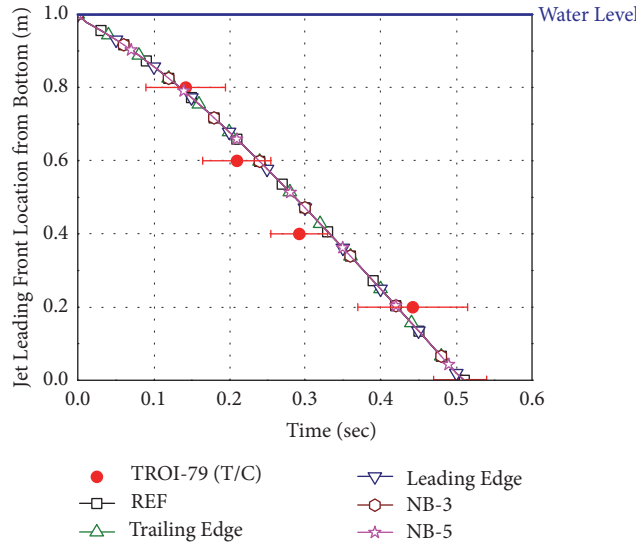

FIGURE 7: Locations of melt jet leading front in TROI experiment and TEXAS-V simulation for the submerged-RV condition with the results of sensitivity analysis.

the variations of the melt front locations. This is because the melt front was ahead of the free particles and fragmented during the total simulation time. In the reference case, the initially scattered particles not shown in the experiment were not simulated, unlike the case for the partially flooded cavity.

In the TROI experimental facility, four K-type thermocouples were installed to measure the water temperature at heights of 0.2, 0.4, 0.6, and 0.8 m in the test section. When the melt jet front reached the bottom of the test section (0.5 s), the increase in water temperature was 0.2 to 1.0 K in the thermocouples. Measurement of the small increase involved high uncertainty owing to the fluctuation of the detection during a short time. About 0.4 K of the water temperature increased at 0.5 s in the simulation. After 1.0 s from the start, about 2.0 K of water temperature increased in both the experiment and simulations owing to the continuous injection of corium into water. Figure 8 shows void fractions in the experiment and TEXAS-V simulation. The void fractions at 0.5 s were not different with the initial values in the experiment. The void fractions slightly increased in the simulation. Due to the small inertia force caused by the small initial velocity, the melt jet gradually accelerated and fell through the water as a lump. A thick vapor film around

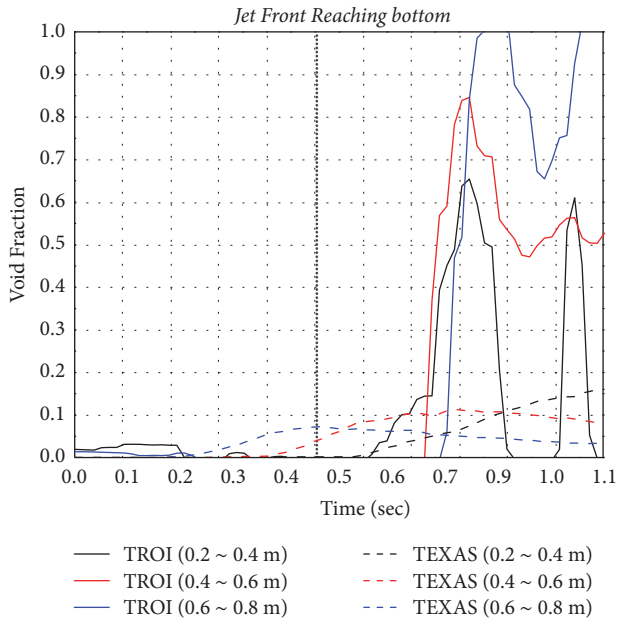

Figure 8: Void fractions in TROI experiment and TEXAS-V simulation for the submerged-RV condition.

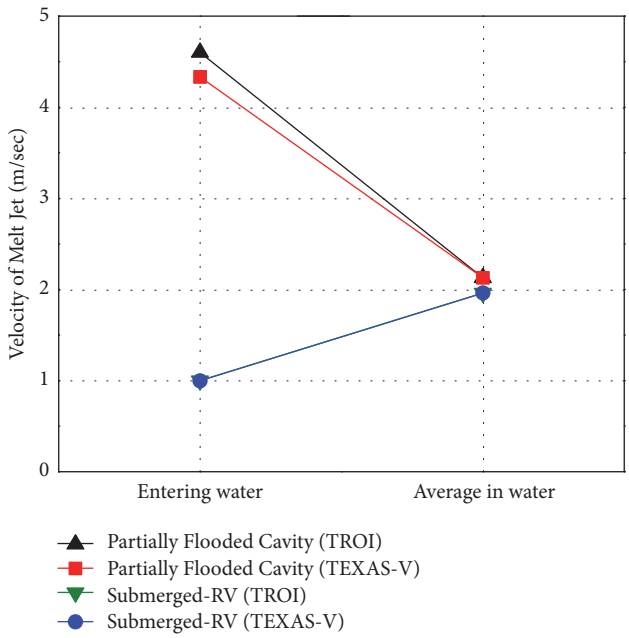

Figure 9: Velocities of melt front in experiments and simulations.

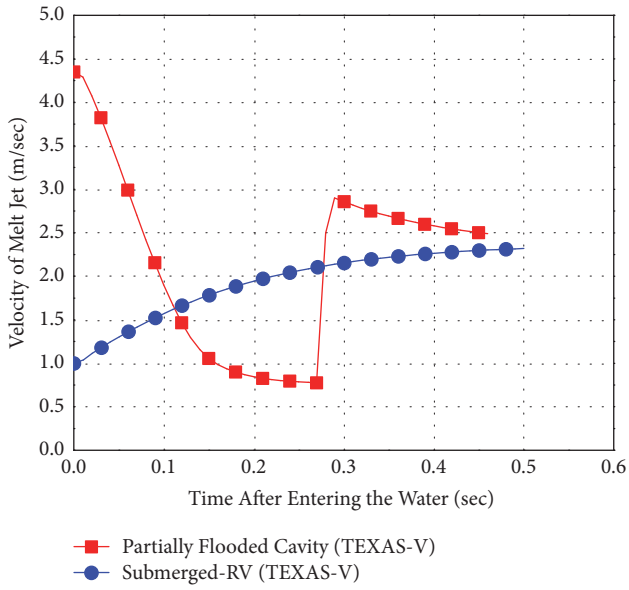

Figure 10: Variation of velocity of melt front through water in TEXAS-V simulation.

the melt stream was observed in the TROI experiment. In addition, because major large steam bubbles were released over the surface of water along the stream of the melt jet in the water, the void fractions were kept low before the bottom impingement of the melt jet. At the time the jet front reached the bottom, the void fraction in the center of the water was 0.0 in the TROI experiment and 0.04 in the TEXAS-V code. After the bottom impingement of the melt jet, void fractions sharply increased at all detected points in the experiments. After 1 s from the injection of the corium, the void fraction in the center of the water was 0.52 in the experiment and 0.09 in the simulation. As the bottom impingement of the corium jet resulting in strong fragmentation was not modeled in the TEXAS-V and the weak fragmentation acted on the large particles through the water, the temperature increase of water was small, and the void fractions were kept low. This does not have any significant effect on the explosion phase owing to the assumption for the bottom contact triggering in the next chapter. For the simulation of the explosion phase, the premixing simulation finishes at the time the melt particles reach the bottom.

3.3. Comparison of Two Conditions. The simulation results for the TROI-68 and TROI-79 are compared below.

A similar tendency in the experiment and simulation for each condition is shown in the previous subchapters. The velocities at which the melt jets enter the water and the average velocities during falling through water under the two conditions are shown in Figure 9. The melt jet was accelerated during a free-fall height of 1 m in the partially flooded cavity condition. The melt jet was almost stopped in the intermediate valve and directly fell into the water. However, it took about 0.5 s for both melt jets to reach the bottom of the water test section. This means one average velocity in the water is similar to the other. As shown in Figure 10, the melt front and the scattered free particles in the partially flooded cavity condition were fragmented from the top of the water. At 0.27 s, the following corium particle overtook the leading edge of the melt jet and started to be fragmented again. The velocity of the melt in the submerged-RV condition gradually increased in the water, as shown in Figure 10. A weak instability at the leading edge resulted in a slow decrease in acceleration. The side of the melt jet was fragmented continuously owing to the KHI.

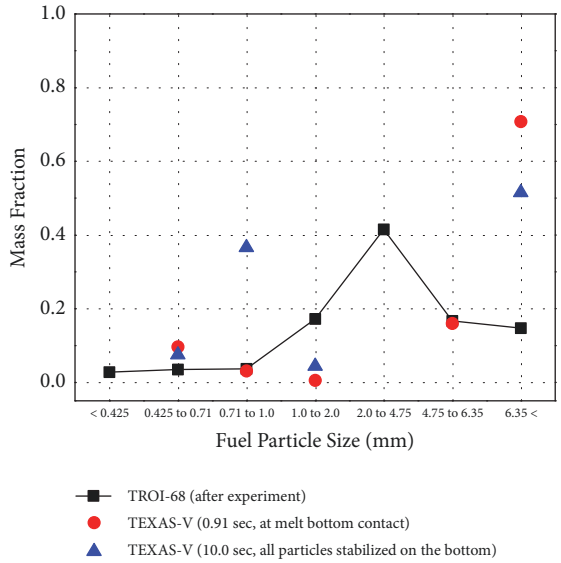

Figure 11: Particle size distribution in the condition for partially flooded cavity.

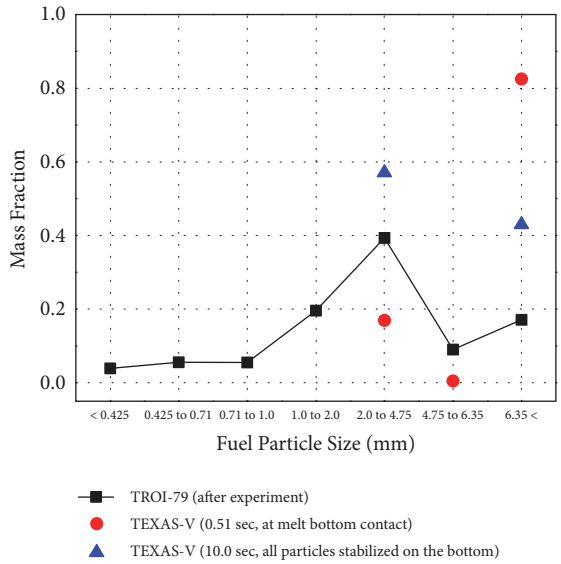

Figure 12: Particle size distribution in the condition for submerged-RV.

Particle size distributions under the two conditions are displayed in Figures 11 and 12. The black lines indicate the data from the TROI experiments. After performing the experiment, the debris accumulated at the bottom of the test section was collected for a postdebris analysis. Then, the debris was sieved and weighed for analyzing the particle size distribution. When comparing the experimental data in TROI-68 and TROI-79, no significant difference appeared. The fractions of the corium particle sizes in the two experiments were high in 2.0 to 4.75 mm. Red dots represent the size distribution when the melt jet reaches the bottom of the water test section during the simulations. These data at this point are used as the initial size distribution in the

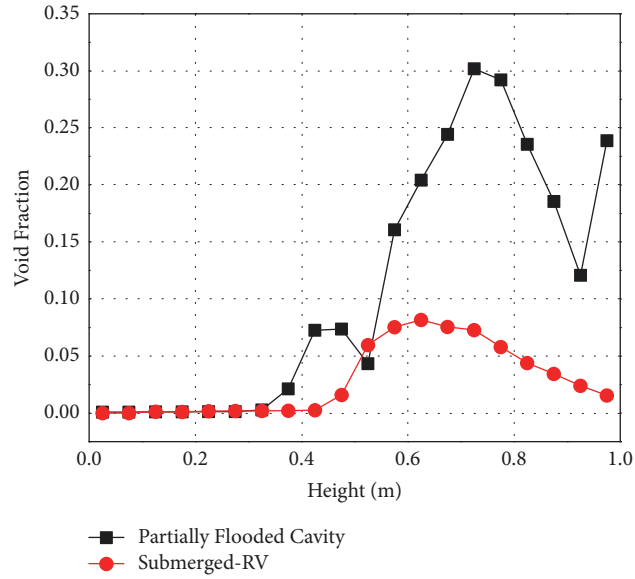

Figure 13: Axial distribution of void fraction at the triggering time in both cases.

simulation of the propagation phase of a steam explosion. The melt front and free particles in the partially flooded cavity condition were fragmented into much smaller sizes than those in the submerged-RV condition. Blue dots represent the size distribution of the corium particles accumulated at the bottom after the injection of all of the corium. Compared with the red dots, the portion of fragmented particles increased. The portion of particles whose size is smaller than 1.0 mm was high in the partially flooded cavity condition, while it did not appear in the submerged-RV condition. The inconsistency in the results between the experiments and the simulations at the end of the test was induced by the effect of the bottom impingement. All particles were fragmented again owing to the bottom impingement in the experiments. Even though more fragmented particles were observed before the time of melt bottom contact in the partially flooded cavity condition than in the submerged-RV condition, the similar size distributions in the two experiments were gathered by sieving the particles after the tests. These were shown in Figures 11 and 12. However, all the particles stopped at the bottom in the simulations when they reached the bottom. The fragmentation from the physical collision on the bottom was not included in the modeling of the simulations.

The axial distributions of the void fractions at the triggering times in both cases are shown in Figure 13. There were more fragmented particles in the partially flooded condition than in the submerged-RV condition as shown in the experiments and simulations. In the experiment for the partially flooded condition, more small bubbles around the corium particles were observed. The more the corium particles were fragmented into smaller particles in the TEXAS-V simulation, the more the heat transfer area between the corium particles and water increased. This caused more vaporization of water on each surface of the corium particles. On the other hand, a thick film was formed around the

surface of the melt jet under the submerged-RV condition because the melt jet stream fell into the bottom as a lump. The heat area between the corium and water in the submerged-RV condition was smaller than that in the partially flooded condition.

The variations in temperatures were not significantly shown in the results of the experiments. This can also be explained by the temperature increase of water. During the same premixing time between the melt jet and water in the two simulation cases, the temperature in the case of the partially flooded condition increased more than that in the case of the submerged-RV condition.

4. Simulations for Explosion Phase

The phases of triggering, propagation, and expansion are simulated by the TEXAS-V code based on the results of the premixing phase under the conditions of a partially flooded cavity and submerged-RV. The occurrence of the bottom triggering is assumed for simulating an ex-vessel steam explosion in a reactor cavity. Therefore, when the lowest melt particle reaches the bottom of the water test section, the calculation for the premixing phase is set to be finished. Accordingly, the defined trigger pressure is imposed on the lowest water cell in the code. The fine fragmentation rate during the explosion phase was calculated in each cell of the TEXAS-V. The void fraction and dynamic pressure were calculated under the assumption that water around each fuel particle was vaporized within a very short time of the propagation phase.

The explosion processes for the conditions of the partially flooded cavity and the submerged-RV were calculated on the basis of the premixing results described in the previous chapter. To analyze the effects of corium entry condition, only the location of the corium injection, which varied the jet velocity at the water level, was changed in the two cases.

The pressure variations calculated at the bottom of the water test section under both conditions are shown in Figure 14. The pressure peak under the partially flooded cavity condition was higher and narrower than that in the submerged-RV condition. As the independent leading particles in the partially flooded cavity condition were strongly fragmented and located at the center of the water at the time of the triggering, the bigger pressure wave was generated and propagated from the center cell. Compared with that, the particle distribution in the submerged-RV condition was quite uniform throughout the water.

The impulse is defined by integrating the calculated dynamic pressure for each time. Under the assumption that a total water above the triggering point is accelerated by a steam explosion upward in one dimension, the water velocity is calculated by a total mass of water. Finally, the kinetic energy converted from the total thermal energy of the melt can be estimated by the water mass and velocity pushed out based on the calculation method proposed in the previous study [18]. The kinetic energy calculated from the pressure variation of the steam explosion is plotted in Figure 15. The kinetic energy in the partially flooded cavity condition was 75.1 kJ, and that

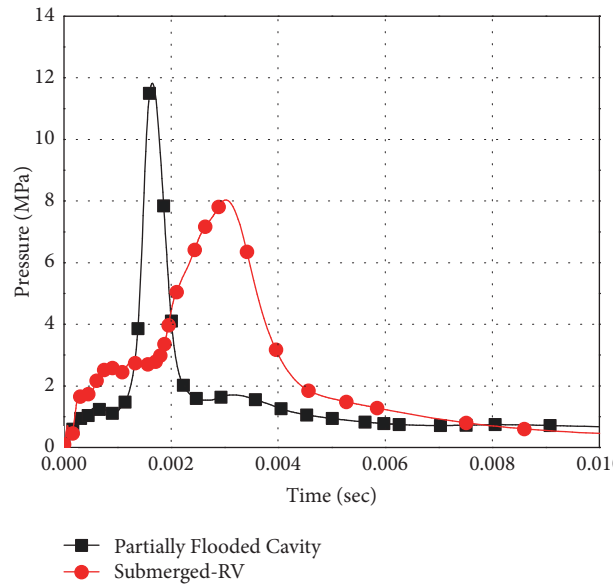

Figure 14: Maximum pressure calculated at the bottom of the water tank in both cases.

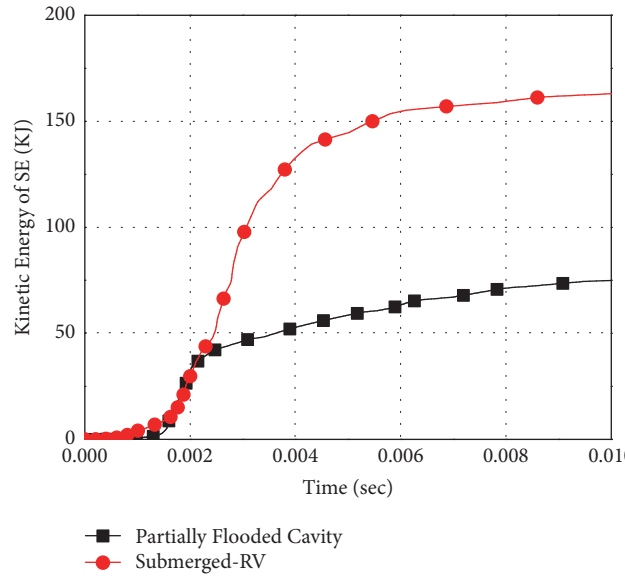

Figure 15: Kinetic energy calculated from the impulse of steam explosion at the bottom of the water tank in both cases.

in the submerged-RV condition was 163.0 kJ. There are two main reasons for the difference between the two values.

Firstly, a larger mass of corium was involved in calculating the total load of the steam explosion in the submerged-RV case than in the partially flooded cavity case. Figure 16 shows the finely fragmented melt mass during the propagation and expansion phases in both cases. Comparing the particle size distributions at the time of triggering shown in Figures 11 and 12, the mass fraction of particles larger than 6.35 mm in the submerged-RV case was higher than that in the partially flooded case. The mass fraction of the melt jet under water was 52.2 % in the partially flooded case, and that was 74.7

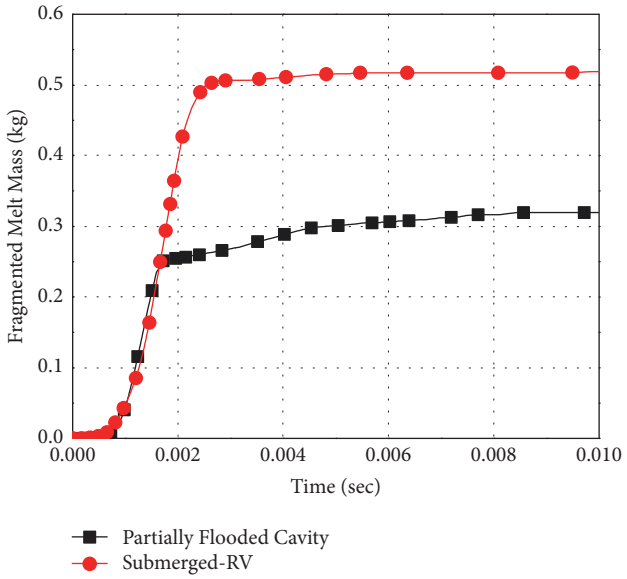

Figure 16: Finely fragmented melt mass during steam explosion in both cases.

% in the submerged-RV case. However, it was found that the mass mean diameter of melt particles at the end of the explosion was 1.0 mm in the partially flooded case, and that was 1.9 mm in the submerged-RV case. Therefore, the total mass of the melt particles, which were finely fragmented in the propagation phase in the submerged-RV case, was bigger than that in the partially flooded cavity. Owing to the continuous propagation of pressure wave during the sufficiently long propagation time, the surfaces of large particles were fragmented into fine particles. Vapor films formed around the finely fragmented particles resulted in the large conversion ratio of the thermal energy to the kinetic energy.

Secondly, void fractions in the partially flooded cavity case were higher than those in the submerged-RV case, as shown in Figure 13. The void fractions at higher positions than 0.55 m in the partially flooded cavity case were higher than those in the submerged-RV case and close to 0.3. When the flow regime changes from a bubbly flow to a slug or droplet flow, the surfaces of corium particles are covered by steam and the direct contact area between corium particles and liquid water decreases significantly. Less vaporization of liquid water by melt particles results in less fragmentation rate in the propagation phase. In the TEXAS-V, a range of the void fraction for the bubbly flow regime is defined. When the void fraction in a fluid cell is higher than the defined value, the generation of steam sharply decreases in the propagation phase. Under partially flooded cavity conditions, the void fractions rose owing to the heat transfer between the fragmented particles and water in the premixing phase. Because there were fewer small fragmented particles in the submerged-RV condition, the temperature and void fraction have risen to a limited extent before the melt bottom contact.

Based on the calculation method proposed by Hong et al., the conversion ratio was calculated by the total thermal energy of the melt under water and the kinetic energy from the steam explosion [18]. The conversion ratio in the partially flooded case is 0.3% and that in the submerged-RV case is 1.0%. Even though a steam explosion is intentionally triggered regardless of the particle size distribution, and the pressure wave from the triggered cell is propagated well to adjacent cells in a one-dimensional code, the conversion ratio in the submerged-RV case is larger than the general value.

5. Conclusions

The reactor cavity of a nuclear power plant may or may not be filled with water at the time of a severe accident according to a severe accident management guideline or the accident conditions. The effects of a free-fall of corium on steam explosion were investigated in this paper. The two premixing experimental tests were simulated by the TEXAS-V code for benchmarking purposes. Based on the results of the premixing phase, the explosion phases in the two cases were simulated. A larger impulse of a steam explosion in the submerged-RV case was calculated than in the partially flooded case. There are two main reasons for this. First, more mass of corium was involved in the submerged-RV case. When a corium jet fell into water without a free-fall height, a weaker inertial force caused a smaller fragmented force in the premixing phase, compared with the case of a partially flooded cavity with a free-fall height. Larger pressure loads were calculated owing to the large sized particles fragmented during the sufficiently long propagation time. Second, as the melt jet fell through water as a lump in the case of the submerged-RV, less steam was produced than in the case of the partially flooded cavity. The distribution of void fractions was similar in both the experiments and simulations. The effect of a large bubble around a melt jet is an important element to be simulated well.

In general, the distribution of smaller corium particles results in a larger impulse of a steam explosion owing to the larger contact area between the corium and water at the end of the premixing phase. However, it was found that the impulse of a steam explosion can be larger in spite of the distribution of larger corium particles when the pressure wave is propagated well in the uniform distribution of corium particles and the low overall void fractions of water.

To analyze the actual plant conditions, the water level and temperature have to be varied in the simulations for the steam explosion. The increase in the water level will result in an increase in the corium mass involved in the explosion. However, it also implies that more particles are fragmented and solidified as the water level increases. In addition, the increase in the initial water temperature will act as a limiting value for the fragmentation during the propagation phase. However, under actual submerged-RV conditions, the water temperature can be stratified if the height of the cavity is high. The water temperature around the bottom of the reactor vessel is saturated owing to the heat transfer from the inside of the reactor vessel. On the other hand, the water temperature in the lower part of the cavity will be lower than the saturation temperature in the initial state. This can cause a larger impulse of the steam explosion owing to the low rate of solidification

of corium particles in the higher part and very low void fraction in the lower part where a steam explosion occurs.

Two steam explosion tests which were carried out with the external triggering in the same TROI facility for the conditions of partially flooded cavity and submerged-RV will be analyzed as a further study of this paper.

Data Availability

The data used to support the findings of this study are available from the corresponding author upon request.

Conflicts of Interest

The authors declare that there are no conflicts of interest regarding the publication of this paper.

Acknowledgments

This work was supported by the National Research Foundation of Korea (NRF) grant funded by the Korea government (Ministry of Science and ICT; Grant no. 2016M2C6A1004893).

References

[1] OECD/NEA, OECD Research Programme on Fuel-Coolant Interaction Steam Explosion Resolution for Nuclear Applications - SERENA, Final Report - December 2006, NEA/CSNI/R(2007)11, 2007.

[2] OECD/NEA, OECD/SERENA Integrated Report (Steam Explosion Resolution for Nuclear Applications), 2014.

[3] R. Meignen, B. Raverdy, M. Buck et al., "Status of steam explosion understanding and modelling," *Annals of Nuclear Energy*, vol. 74, no. C, pp. 125–133, 2014.

[4] OECD/NEA, Status Report on Ex-Vessel Steam Explosion: EVSE, OECD/NEA /CSNI/R(2017)15, March, 2018.

[5] Y. Li, Z. Wang, M. Lin, M. Zhong, Y. Zhou, and Y. Yang, "Experimental Studies on Breakup and Fragmentation Behavior of Molten Tin and Coolant Interaction," *Science and Technology of Nuclear Installations*, vol. 2017, 14 pages, 2017.

[6] M. Zhong, Y. Li, M. Lin, M. Yuan, and Y. Yang, "A Numerical Analysis Research on Earlier Behavior of Molten Droplet Covered with Vapor Film at the Stage of Triggering and Propagation in Steam Explosion," *Science and Technology of Nuclear Installations*, vol. 2014, 10 pages, 2014.

[7] K. Moriyama and H. S. Park, "Probability distribution of ex-vessel steam explosion loads considering influences of water level and trigger timing," *Nuclear Engineering and Design*, vol. 293, pp. 292–303, 2015.

[8] K. Moriyama and H. S. Park, "Parameter dependence of steam explosion loads and proposal of a simple evaluation method," *Nuclear Engineering and Technology*, vol. 47, no. 7, pp. 907–914, 2015.

[9] M. L. Corradini et al., *User's Manual for TEXAS: One Dimensional Transient Fluid Model for Fuel-Coolant Interaction Analysis*, University of Wisconsin, Madison, Wis, USA, 2012.

[10] J. Tang, *Modeling of the Complete Process of One-Dimensional Vapor Explosions [Thesis paper]*, 1993.

[11] M. L. Corradini et al., *Fuel-Coolant Interaction Analyses with TEXAS-V Vapor Explosion Model*, University of Wisconsin, Madison, Wis, USA, 1999.

[12] A. Annunziato, A. Yerkess, and C. Addabbo, "FARO and KROTOS code simulation and analysis at JRC Ispra," *Nuclear Engineering and Design*, vol. 189, no. 1-3, pp. 359–378, 1999.

[13] R. Chen, J. Wang, G. H. Su, S. Qiu, and M. L. Corradini, "Analysis of KROTOS KS-2 and KS-4 steam explosion experiments with TEXAS-VI," *Nuclear Engineering and Design*, vol. 309, pp. 104–112, 2016.

[14] H. J. Song, I. Park, and J. H. Kim, "A Coherent Methodology for the Evaluation of a Steam Explosion Load Using TEXAS-V," *Journal of the Korean Nuclear Society*, vol. 6, no. 36, pp. 571–581, 2004.

[15] KAERI, "The Coherent Evaluation of the Steam Explosion Load by Using TEXAS-V," Korea Atomic Energy Research Institute, KAERI/TR-3066/2005, 2005.

[16] S. W. Hong, Y. S. Na, S. H. Hong, and J. H. Song, "Fuel-coolant interaction test results under different cavity conditions," *Nuclear Technology*, vol. 196, no. 3, pp. 538–552, 2016.

[17] Y. S. Na, S.-H. Hong, J. H. Song, and S.-W. Hong, "Fuel–Coolant Interaction Visualization Test for In-Vessel Corium Retention External Reactor Vessel Cooling (IVR-ERVC) Condition," *Nuclear Engineering and Technology*, vol. 48, no. 6, pp. 1330–1337, 2016.

[18] S. W. Hong, "Conversion ratio of molten corium in TROI steam explosion experiment," in *Proceedings of the Transactions of the Korean Nuclear Society Spring Meeting*, Jeju, Korea, 2017.